DOI: 10.1002/ejic.201100110

$Ag_3(SO_3F)_4$: A Rare Example of a Mixed-Valent Ag^{II}/Ag^{I} Compound Showing 1D Antiferromagnetism

Tomasz Michałowski,[a] Przemysław J. Malinowski,[a] Mariana Derzsi,[b] Zoran Mazej,[c] Zvonko Jagličić,[d] Piotr J. Leszczyński,[b] and Wojciech Grochala*[a,b]

Dedicated to Professor Boris Žemva on the occasion of his 70th birthday

Keywords: Silver / Mixed-valent compounds / Density functional calculations / Fluorosulfate

Dark brown $Ag^{I}_2Ag^{II}(SO_3F)_4$, known for over 30 years, is the first known example of four well-characterized mixed-valent (1+/2+) compounds of silver. It crystallizes in the monoclinic space group, $P2_1/c$, with a = 5.33670(19) Å, b = 12.9486(4) Å, c = 19.5976(7) Å, β = 100.6407(13)°, V = 1330.95(8) Å^3, Z = 4 and $d_{calcd.}$ = 3.59 g cm^{-3}. Its chemical formula is best written as $[Ag^{I}_2(SO_3F)]^+[Ag^{II}(SO_3F)_3]^-$. Ag^{II} centres form 1D chains linked through OSO bridges that result in pronounced antiferromagnetic coupling with T_N = 225 K and a superexchange coupling constant (J) of –7.5 meV per pair of coupled Ag^{II} cations. Ligand environments around Ag^{I} and Ag^{II} differ substantially, which suggests a genuine mixed- (i.e., localized) and not intermediate-valent (i.e., delocalized) character of the title compound. Indeed, electronic absorption is not observed up to 7500 cm^{-1}, so the intervalence charge-transfer transition across the electronic band gap must fall above 0.8 eV. The compound is stable up to a mere 75 °C, which marks the onset of its thermal decomposition to $Ag^{I}SO_3F$ and the $SO_3F^{\cdot}$ radical. $Ag^{I}_2Ag^{II}(SO_3F)_4$ is, after $AgSO_4$, the second-known 1D antiferromagnetic semiconducting oxa derivative of Ag^{II}.

Introduction

Very little is known about mixed-valent Ag^{I}/Ag^{II} compounds. At the time of writing only three examples[1] of such compounds have been described in the literature:

1. silver(I,II) fluorosulfate,[2] $Ag^{I}_2Ag^{II}(SO_3F)_4$ (the title compound, claimed to be black)
2. two dark red complexes of Ag^{I} acetylide and Ag^{II} with tetramethylcyclam,[3,4]
3. green silver(I,II) hexafluoroantimonate(V),[5] $Ag^{I}_2Ag^{II}(SbF_6)_4$.

Historically the first among these, $Ag^{I}_2Ag^{II}(SO_3F)_4$, briefly described by Leung and Aubke in 1978,[2] seems to be most interesting as its dark colour is indicative of low-energy electronic transitions, such as intervalence charge-transfer (IVCT) excitations expected for compounds exhibiting mixed valence. Black is often indicative of a narrow energy gap at the Fermi level and the possibility of achieving metallization either by means of doping or by applying external pressure. As compounds containing highly oxidizing Ag^{II} species may exhibit unusual electronic and magnetic properties (as in the case of black semiconducting $AgSO_4$[6]) and possibly even superconductivity,[7] detailed examination of the title compound was desired. Here we report the crystal structure of $Ag^{I}_2Ag^{II}(SO_3F)_4$ as well as its 1D antiferromagnetism, similar to that of $AgSO_4$.[6]

[a] Faculty of Chemistry University of Warsaw,
Pasteur 1, 02093 Warsaw, Poland
Fax: +48-22-5540801
E-mail: wg22@cornell.edu
[b] Interdisciplinary Center for Mathematical and Computational Modelling, University of Warsaw,
Pawinskiego 5a, 02106 Warsaw, Poland
[c] Department of Inorganic Chemistry and Technology, Jožef Stefan Institute,
Jamova 39, 1000 Ljubljana, Slovenia
[d] University of Ljubljana, Faculty of Civil and Geodetic Engineering, and Institute of Mathematics, Physics and Mechanics,
Jadranska 19, 1000 Ljubljana, Slovenia

Results and Discussion

A mixed-valent silver(I)–silver(II) fluorosulfate can be synthesized by using a number of methods. It can be obtained by treating a mixture of AgF and AgF_2 (2:1 molar ratio) with an excess amount of sulfur trioxide, see Equation (1).

$$2AgF + AgF_2 + 4SO_3 \rightarrow Ag^{I}_2Ag^{II}(SO_3F)_4 \quad (1)$$

Alternatively, it can be obtained from the reaction between AgF_2 and HSO_3F in which silver(II) fluorosulfate is first formed according to Equation (2).

$$AgF_2 + 2HSO_3F \rightarrow 2HF\uparrow + Ag(SO_3F)_2 \quad (2)$$

and then slowly decomposes to give $Ag^{I}_2Ag^{II}(SO_3F)_4$ according to Equation (3).

$$3Ag(SO_3F)_2 \rightarrow Ag_3(SO_3F)_4 + (SO_3F)_2 \quad (3)$$

This pathway is very time-consuming, but after four months the solid residue contains approximately 88.6 wt.-% of the mixed-valent compound, still contaminated with AgF_2 and $Ag(SO_3F)_2$. Remnants of acid may be removed by heat treatment at 60 °C for 0.5 h.

The highest purity samples of $Ag^{I}_2Ag^{II}(SO_3F)_4$ of quality appropriate for magnetic studies were obtained by treating silver(I) fluorosulfate with bromine(I) fluorosulfate according to the published procedure, see Equation (4).[2]

$$3AgSO_3F + BrSO_3F \rightarrow Ag^{I}_2Ag^{II}(SO_3F)_4 + 1/2Br_2 \quad (4)$$

All chemical and physical properties (except for crystal structure refinement) reported below are for the samples synthesized according to Equation (4). The elemental content for these samples is shown in Table 1, as compared with theoretical values for mixed-valent silver(I,II) fluorosulfate as well as fluorosulfates of silver(I) and silver(II).

Table 1. Elemental content analysis (Ag, S and F) for $Ag_3(SO_3F)_4$.

Element	Exp. $[Ag_3(SO_3F)_4]$	Theor. $[Ag_3(SO_3F)_4]$	Theor. $(AgSO_3F)$	Theor. $[Ag(SO_3F)_2]$
Ag	45.9	45.0	52.2	35.3
F	10.9	10.6	9.2	12.4
S	17.5	17.8	15.4	20.9

All results are within the error margins of the methods applied. The results suggest that $Ag^{I}_2Ag^{II}(SO_3F)_4$ was indeed obtained.

Crystal Structure: 1D $Ag^{II}(SO_3F)^+$ Chains Linked into 2D $Ag^{II}(SO_3F)_3^-$ Sheets and Isolated $Ag^{I}_2(SO_3F)^+$ Cations

The best-quality powder X-ray diffractogram was obtained for the sample synthesized over four months from the reaction between AgF_2 and HSO_3F, see Equations (2) and (3). The pattern obtained is shown in Figure 1 together with the differential curve from three-phase refinement of the structure. The sample was found to contain 1.5 wt.-% AgF_2 and 9.9 wt.-% $Ag(SO_3F)_2$. For these two impurities only the unit-cell parameters were refined. Soft restrictions on bond lengths and angles of the SO_3F^- anions were applied as described before.[8] The structure of $Ag^{I}_2Ag^{II}(SO_3F)_4$ was solved by using Jana2006[9] combined with Expo2004,[10] which provided the starting model for the refinement.

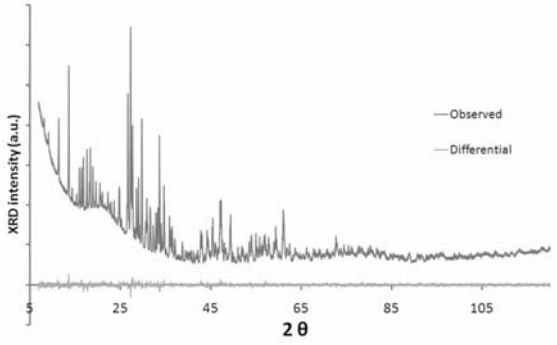

Figure 1. Experimental X-ray powder diffractogram of $Ag^{I}_2Ag^{II}(SO_3F)_4$ and the differential curve. For decomposition of the observed pattern into particular components, see the Exp. Sect.

Two projections of the crystal structure are shown in Figure 2. The refined unit-cell parameters and selected interatomic contacts are listed in Table 2. $Ag^{I}_2Ag^{II}(SO_3F)_4$

Table 2. Unit-cell and refinement parameters and selected bond lengths for $Ag^{I}_2Ag^{II}(SO_3F)_4$.

Space group	$P2_1/c$		T	298 K
V [Å^3]	1330.95(8)		Z	4
a [Å]	5.33670(19)		R_p	0.0153
b [Å]	12.9485(4)		R_{wp}	0.0200
c [Å]	19.5976(7)		$R_{(Bragg)}$	0.0228
β [°]	100.6407(13)		GOF	1.50
Ag^{II}–O	2.055(18)	2.13(2)	2.424(17)	
	2.07(2)	2.15(2)	2.609(17)	
Ag^{I}a–O	2.26(2)	2.460(19)	2.718(19)	2.843(16)
	2.36(2)	2.669(18)	2.82(2)	
Ag^{I}b–O	2.34(2)	2.49(2)	2.648(18)	
	2.446(16)	2.52(2)	2.78(2)	

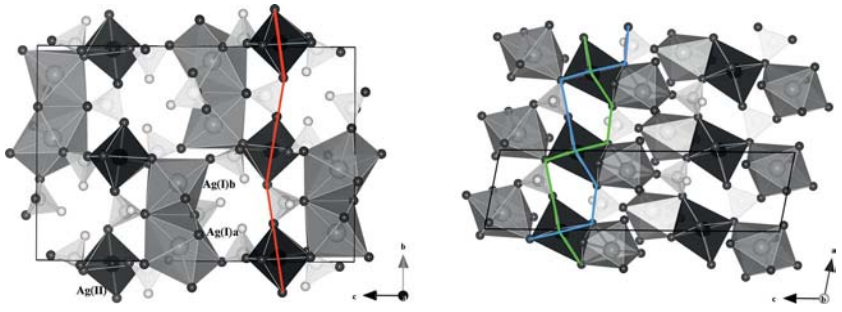

Figure 2. Two projections of the unit cell of $Ag^{I}_2Ag^{II}(SO_3F)_4$ emphasizing SO_3F tetrahedra (light grey), $Ag^{II}O_6$ octahedra (dark grey) and two different Ag^{I} coordination spheres (octahedron and pentagonal bipyramid: medium grey). Left: projection on the *bc* plane emphasizing the presence of 1D $[Ag^{II}(SO_3F)_{2/2}]^+$ chains (printed in red) and of $Ag^{I}_2(SO_3F)^+$ cations. Right: projection on the *ac* plane emphasizing the links between successive $[Ag^{II}(SO_3F)_{2/2}]^+$ chains (generated with VESTA[15]).

crystallizes in the monoclinic space group $P2_1/c$ with large values of ***b*** and ***c*** vectors, which lead to a unit-cell volume exceeding 1300 Å^3. There are three nonequivalent Ag atoms in the structure of which two are Ag^I (hereafter referred to as Ag^Ia and Ag^Ib) and one is Ag^{II}.

The Ag^{II} cations are coordinated by six O atoms arranged into a deformed elongated octahedron with four short [2.055(18), 2.07(2), 2.13(2), 2.15(2) Å] and two long bond lengths [2.424(17), 2.609(17) Å]. The average Ag^{II}–O distance is 2.24(2) Å. The Ag–O distances are very similar to those found for $Ag(SO_3F)_2$ [$2\times2.07(3)$ Å, $2\times2.154(19)$ Å and $2\times2.49(2)$ Å, i.e., 2.24(2) Å on average; and $2\times2.053(18)$ Å, $2\times2.14(3)$ Å and $2\times2.61(2)$ Å i.e., 2.27(2) Å on average]. The dimensionless parameter of Jahn–Teller distortion, *D*,[11] takes the value of 1.194, which is comparable to those of 1.179–1.245 seen for $Ag^{II}(SO_3F)_2$.[8] The Ag^{II} cations are linked through O–S–O bridges into 1D $Ag^{II}(SO_3F)^+$ chains propagating along *b* with an O–Ag–O angle of 176.4(11)° and Ag–O–O angles of 176.6(5) and 162.4(5)°. This close to linear geometry of the Ag···OO···Ag bridge has major consequences for magnetic properties of the compound (see below). The $Ag^{II}(SO_3F)^+$ chains are further polymerized along *a* into 2D $Ag^{II}(SO_3F)_3^-$ sheets using two additional SO_3F^- anions.

As for the Ag^I cations, the first coordination sphere is in the form of a deformed pentagonal bipyramid for Ag^Ia and of a deformed octahedron for Ag^Ib. In the bipyramid the apical O atoms are the nearest to the transition-metal atom. An average Ag–O distance is 2.59 Å for Ag^Ia, and 2.54 Å for Ag^Ib. Accordingly, the bond-valence sum[12]for Ag^Ia [1.10(3)] is larger than that for Ag^Ib [0.99(2)]. The AgO distances are similar to those found for $Ag^I(SO_3F)$[13] with a deformed octahedral coordination of Ag^I [an average of 2.54(2) Å].

There are four independent SO_3F^- anions in the structure. The first SO_3F unit (S1) bridges Ag^{II} cations through an OSO linker. The other two SO_3F units (S2, S3) bridge Ag^{II} with Ag^{II} and Ag^{II} with Ag^I cations also utilizing the OSO links. The last SO_3F unit (S4) bridges only pairs of Ag^I cations using both –O– and –OSO– linkers, just like that seen for Ag^ISO_3F.[13] The presence of SO_3F^- anions that are not attached to Ag^{II} suggests the formulation of the compound as $[Ag^I_2(SO_3F)]^+[Ag^{II}(SO_3F)_{4/2+2/2}]^-$. The $Ag^I_2(SO_3F)^+$ cations are located between the $[Ag^{II}(SO_3F)_{4/2+2/2}]^-$ sheets. The first type of fluorosulfate anions has one terminal O and one terminal F atom (by terminal atom we mean here one that is not bound strongly to Ag^{II}); terminal O is used for bridging between Ag^Ia and Ag^Ib. The second type of fluorosulfate anion has one terminal O and one terminal F. Here the terminal O atom is used for weak (secondary) bonding to Ag^{II}, while completing its coordination sphere from square-planar to elongated octahedral. For the last type of fluorosulfate anion in which all O atoms are involved in bonding to Ag^I, only F atoms are terminal. In summary, none of the fluorine atoms are bound to a metal cation [such binding occasionally occurs in fluorosulfates, for example for $Ti_3Cl_{10}(SO_3F)_2$[14] or for $AgSO_3F$[13]]. Similarly to what is found in $Ag(SO_3F)_2$,[8] F atoms form narrow channels along the *a* crystallographic axis.

One might consider a hypothetical Lewis acid/Lewis base reaction between $Ag(SO_3F)_2$ and $AgSO_3F$, see Equation (5).

$$2AgSO_3F + Ag(SO_3F)_2 = Ag_3(SO_3F)_4 \quad (5)$$

The differential volume of reaction [Equation (5)] is –27.94 Å^3 per formula unit, which corresponds to a volume drop of a –2% compared with the expected value. The similarity of the average Ag^{II}–O and Ag^I–O bond lengths compared to those found for the $Ag(SO_3F)_2$ and $AgSO_3F$ precursors testify that Lewis acidities of both pseudobinary fluorosulfates are not vastly different.

Vibrational Spectra as a Fingerprint of Bonding

Comparison of the far- and mid-infrared spectra measured for $Ag^I_2Ag^{II}(SO_3F)_4$ and for two reference compounds, $Ag(SO_3F)_2$ and $AgSO_3F$, is shown in Figure 3. The IR absorption and Raman scattering spectra of $Ag^I_2Ag^{II}(SO_3F)_4$ are shown jointly in Figure 4. Bands appearing in the spectra were assigned to characteristic vibrational modes based on the data from the literature,[16] as listed in Table 3 together with the bands typical for the reference compounds.

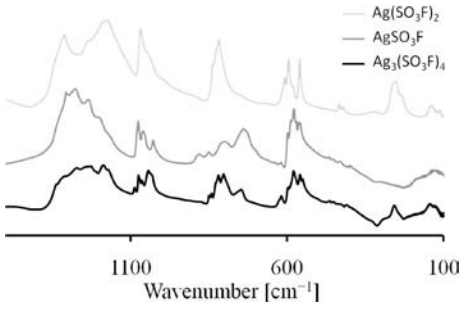

Figure 3. Infrared absorption spectra of $Ag^I_2Ag^{II}(SO_3F)_4$, $Ag(SO_3F)_2$ and $AgSO_3F$.

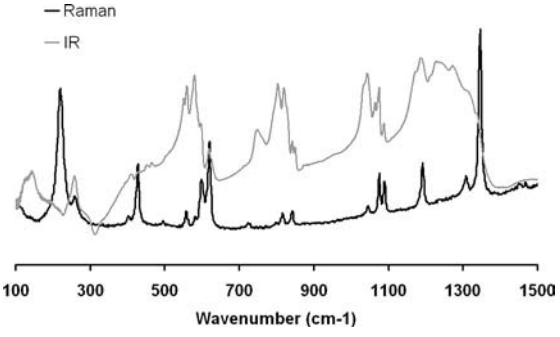

Figure 4. Infrared absorption and Raman scattering spectra of $Ag^I_2Ag^{II}(SO_3F)_4$.

The IR spectrum of $Ag^I_2Ag^{II}(SO_3F)_4$ is similar to those of $AgSO_3F$ and $Ag(SO_3F)_2$ (Figure 3), but clearly not their simple superposition. The spectrum is complex and consists of many bands in all spectral ranges due to the structural complexity of the compound and the large size of the unit

Table 3. Assignment of infrared- and Raman-active bands of $Ag^{I}_2Ag^{II}(SO_3F)_4$ relative to $Ag^{II}(SO_3F)_2$ and $Ag^{I}SO_3F$ and to literature data.[a]

Raman $Ag_3(SO_3F)_4$	Raman $Ag(SO_3F)_2$[8]	IR $Ag_3(SO_3F)_4$	IR (product AgF_2 + $2SO_3$)	IR (lit.) $Ag_3(SO_3F)_4$[2]	IR (lit.) $Ag(SO_3F)_2$[8]	IR (lit.) $AgSO_3F$[13]	Assignment
1347 vs	1340 s	1335 w, sh			1320 w, sh		SO_3 str
1309 mw	1309 w	1311 s, sh	1311 s	1325 s, sh	1313 s	1310 s, br., sh	
		1273 m	1275 m, sh	1278 s			
	1239 vw	1229 m, sh	1226 m, sh	1235 s		1250 s, br.	
1194 m	1194 vw	1188 s		1195 s	1188 s, sh		
	1134 s	1173 m, sh	1171 s, sh		1176 vs, br.		
1089 m	1086 w	1089 w		1095 w			
1075 m	1069 s	1076 s		1082 ms	1070 s	1075 s,sh	
		1065 w	1067 s			1062 s	
1046 w		1044 s, sh	1044 s, sh	1055 s	1046 m, sh		
		850 w	850 vw				SF str
843 w	838 s	843 w	837 m, sh		838 w		
815 w	819 vw	821 s,sh	816 s	830 s	826 w, sh		
		804 s	804 m, sh	810 s	820 s	795 s	
727 vw		748 s				748 s	
620 s		620 s,sh			615 w, sh		SO_3F def
600 m	604 w		609 w, sh		608 m		
	598 s	598 s	594 m		595 m	595 s,sh	
585 vw	587 s	582 s	581 m			587 s, 577 s	
560 w	558 s	560 s, 552 s	559 s, sh		560 m	561 s,sh	
497 vw	434 s	466 w					SO_3F rock
	428 s	435 vw			434 w		
428 m	415 vw	430 vw			421 w		
402 w	410 w	412 w				410 vs	
		394 vw				395 vw	
260 w	238 vs	258 s					Ag–O str & lattice
220 s	219 vs	144 s					
	141 w	127 w,sh					
	118 w						
	91 m						
	78 w						

[a] v: very, s: strong, m: medium, w: weak, br.: broad, sh: shoulder. str = stretching, def = deformation, rock = rocking.

cell. The obtained IR spectrum shows great similarity to the one published by Aubke[2] (with a systematic downshift by 7 cm^{-1} – occasionally larger – likely due to incorrect zero shift in the previous data[2]) and it also bears a strong resemblance to that measured for the product of the highly exothermic reaction between AgF_2 and $2SO_3$.[13]

The S–O stretching region (1000–1350 cm^{-1}) in the IR spectrum is extremely broad and consists of many overlapping bands, clearly as a result of a variety of S–O interactions and of engagement of O in primary and secondary bonding to silver cations at different oxidation states. Presence of IR absorption above 1300 cm^{-1} testifies that at least one oxygen of the fluorosulfate anions is engaged in secondary bonding to silver. The anions may be considered to be (2+1)-dentate. The S–F stretching range (750–850 cm^{-1}) is also rich in bands owing to the presence of four nonequivalent SO_3F groups in the structure and to coupling between oscillators of similar frequency.[17] The S–F band split is revealed in the Raman spectra as well (a sharper band at 842 cm^{-1} and a broader and weaker band at 819 cm^{-1}). The regions of IR absorption due to SO_3F deformations (550–620 cm^{-1}) and rocking (390–470 cm^{-1}) are rich in bands; the Ag–O stretching and lattice modes appear below 260 cm^{-1}.

ESR Spectra and Magnetic Properties

The ESR spectra were measured in the 2.6–296 K temperature range. A very broad line, typical of an ordered magnetic phase, with a *g* factor of approximately 2.119 is evident in the spectrum recorded at room temperature (Figure 5, inset). This is consistent antiferromagnetism of $Ag_3(SO_3F)_4$, which persists at room temperature (Figure 6). At 2.6 K a complex fine structure develops, reminiscent of that for a paramagnetic specimen (Figure 5) but very different from the one measured at 2.6 K for $Ag(SO_3F)_2$.[8] Since all Ag^{II} atoms are equivalent in the cell, a fine structure is due to either a rhombic *g* tensor [recollect a (2+2+2) coordination of Ag] or even due to the coupling between electronic and nuclear spins.

The presence of Ag^{II} with its unpaired 4d electron implies magnetic interactions between Ag^{II} centres. Indeed, the plot of magnetic susceptibility versus temperature (Figure 6) indicates the presence of a broad maximum of susceptibility at 225 K (cf. the previously reported value of 240 K[2]). $Ag^{I}_2Ag^{II}(SO_3F)_4$ is thus proven to order antiferromagnetically, similarly to $AgSO_4$.[6] 1D antiferromagnetism persists till approximately 400 K; measurements at

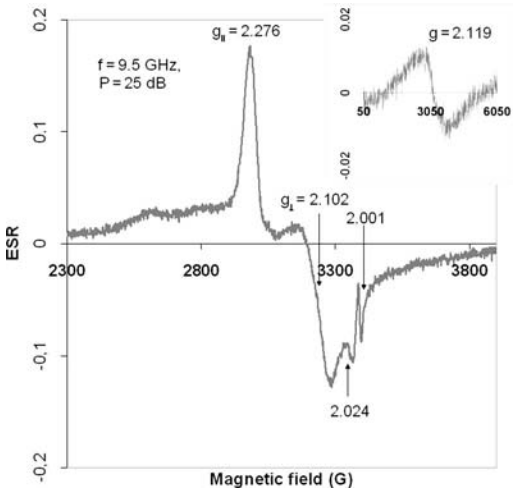

Figure 5. The ESR spectrum of $Ag^{I}_{2}Ag^{II}(SO_3F)_4$ at 2.6 K. Inset: the spectrum measured at 296 K.

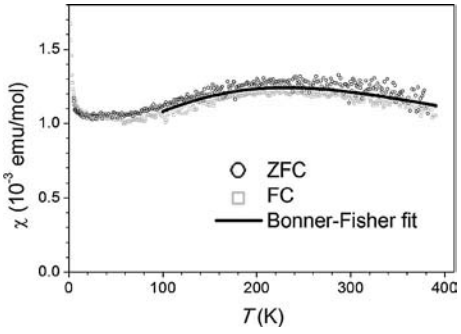

Figure 6. Plot of magnetic susceptibility (χ) versus temperature (T) for $Ag^{I}_{2}Ag^{II}(SO_3F)_4$ (FC: field-cooled regime, ZFC: zero-field-cooled regime).

higher temperatures were not performed due to thermal decomposition of the sample. The Bonner–Fischer model of a 1D antiferromagnet[18] with g = 2.119 taken from ESR spectra (cf. above) gives the exchange integral (J) as –179 K (i.e., –7.5 meV per pair of Ag^{II} cations).

Appearance of strong 1D antiferromagnetic (AFM) coupling is explained by analysis of the crystal structure and well reproduced by DFT calculations (see the next section). The $|J|$ value for $AgSO_4$ (217 K) is approximately 20% larger than that for $Ag^{I}_{2}Ag^{II}(SO_3F)_4$, as also reflected by the positions of the magnetic susceptibility maxima (264 and 225 K, respectively).

DFT Picture of Bonding and Magnetism

To understand the nature of the magnetism and electronic structure of $Ag_3(SO_3F)_4$ we have carried out DFT calculations using local spin density approximation (LSDA) and LSDA+U methods. The electronic band structure and atomic electronic densities of states (dos) are shown in Figure 7; a projection of the spin density within the crystallographic unit cell is presented in Figure 8. Magnetic moments on atoms are listed in Table 4.

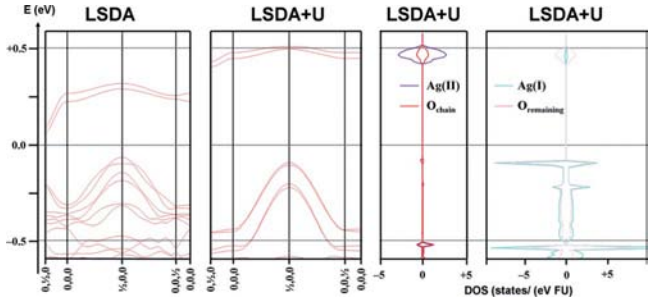

Figure 7. Far left: band structure for $Ag^{I}_{2}Ag^{II}(SO_3F)_4$ as calculated with LSDA; middle left: band structure as calculated with LSDA+U; middle right: partial DOS jointly for all Ag^{II} cations and for O atoms from OSO bridges between Ag^{II} centres (LSDA+U); far right: partial DOS jointly for all Ag^{I} cations and for remaining O atoms (LSDA+U). Colour code for partial DOS is shown. The Fermi level was set to zero.

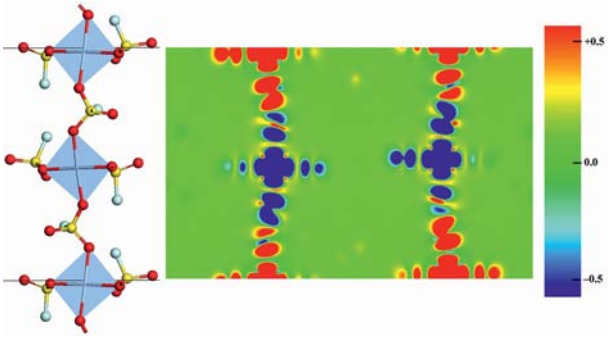

Figure 8. Projection of spin density, ρ_{sp}, as calculated at the LSDA+U level onto the *bc* plane of the crystallographic unit cell of $Ag^{I}_{2}Ag^{II}(SO_3F)_4$ reflecting the antiferromagnetic superexchange within the $[Ag^{II}(SO_3F)_{2/2}]^{+}$ chains (shown on the left). Colour scale [e Å^{-3}] from blue (excess amount of spin down) to red (excess amount of spin up).

Table 4. The magnetic moments on atoms as calculated for the AFM ground state of $Ag_3(SO_3F)_4$ at the LSDA+U level.

Atom	μ [μ_B]	Atom	μ [μ_B]
Ag^{I}a, Ag^{I}b	±0.01	O ($OSO_{intrachain}$)	±0.08
Ag^{II}	±0.49	O ($OSO_{interchain}$)	±0.04 to ±0.05
S, F	0.00	O (not bound to Ag^{II})	±0.00 to ±0.03

Atomic contributions from Ag^{II} and Ag^{I} to the density of states are firmly separated in the energy scale, with Ag^{I} states predominating the valence band and Ag^{II} states constituting the conduction band (Figure 7). This feature confirms the genuine mixed-valent Ag^{I}/Ag^{II} character of the title compound, deduced before from the crystal structure. The 2p states from O atoms of the OSO bridges are substantially mixed up with the 4d states of Ag over the entire energy range ("covalence"[19]). As expected, $Ag_3(SO_3F)_4$ is a Mott–Hubbard insulator, in contrast to $Ag^{II}(SO_3F)_2$ (a charge-transfer insulator).[8] Introduction of the Mott–Hubbard U is not necessary, however, to open the band gap at the Fermi level (Figure 7). A small direct electronic band gap of approximately 0.35 eV appears at (1/2 0 0) even in

the LSDA calculations but it increases to ca. 0.6 eV upon inclusion of the *U* factor. The smallest indirect band gap is approximately 0.5 eV. A more precise estimate of the band gaps requires full optimization of the crystallographic unit cell.

Presence of the 1D $[Ag^{II}(SO_3F)_{2/2}]^+$ chains bridged into $[Ag^{II}(SO_3F)_{4/2+2/2}]^-$ sheets in the crystal structure of $Ag_3(SO_3F)_4$ (see Figures 2 and 8) determines the magnetic behaviour of this compound. The lowest-energy solution is antiferromagnetic within the $[Ag^{II}(SO_3F)_{2/2}]^-$ chains but ferromagnetic between the neighbouring chains.[20] The pathway of the strongest magnetic superexchange between two neighbouring Ag^{II} centres goes via the OO bridge, as in the case of $AgSO_4$.[6,21] Antiferromagnetism of $Ag_3(SO_3F)_4$ thus arises from superexchange of unpaired Ag(4d) electrons residing at x^2–y^2 orbitals (localized within mutually inclined $[AgO_4]$ squares) (Figure 8). The calculated *J* value (–21.4 meV GGA+U, –23.8 meV LSDA+U) is 2 to 3 times overestimated with respect to the experimental value of –7.5 meV, partly due to the fact that the experimental crystal structure was used for calculations without any structural optimization. The values of magnetic moments on Ag^{II} atoms as obtained from the LSDA+U calculations (Table 4) are $\pm 0.49\ \mu_B$, and thus are similar to those calculated for antiferromagnetic $AgSO_4$ (± 0.43–$0.45\ \mu_B$).[6] Simultaneously, the calculated magnetic moments on the bridging O atoms vary between $\pm 0.08\ \mu_B$ (for O atoms within the chain) and $\pm 0.05\ \mu_B$ (for O atoms from fluorosulfate anions that bridge the infinite chains together). The values of magnetic moments on Ag^{I} cations, and on S, O and F atoms coming from fluorosulfate anions that bridge Ag^{I} centres, are negligibly small, as expected.

The appearance of substantial magnetic moments on selected oxygen atoms is equivalent to the partial introduction of holes into O(2p) states (they attain "free radical" character) which – as we will see in the next section – contributes to facile thermal decomposition of $Ag_3(SO_3F)_4$ by means of a redox process.

Thermal Stability

Thermal behaviour of $Ag^{I}_2Ag^{II}(SO_3F)_4$ was studied with thermogravimetric analysis (TGA)/differential scanning calorimetry (DSC)/evolved gas analysis (EGA). The TGA/DSC plots are shown in Figure 9. Thermal decomposition is a two-step process (I: 75–180 °C; II: 180–500 °C) with an onset at temperatures as low as 75 °C. The first step of decomposition accounts for about 7.2 wt.-% whereas the second one for about 16.2 wt.-% mass loss.

The DSC curve is complex, with one broad endothermic peak around 80 °C of uncertain origin [probably evaporation of traces of the $(SO_3F)_2$ substrate occluded in the sample], a broad exothermic peak at 140 °C corresponding to the first step of thermal decomposition (with an overlapping sharp endothermic peak at 155 °C corresponding to melting of $Ag^{I}SO_3F$[13]) and a large distinct endothermic peak at 424 °C corresponding to a structural phase transition of Ag_2SO_4 (orthorhombic → hexagonal, lit. 425 °C).[22] Exothermicity of the first step of the thermal decomposition and evolution of the volatile SO_3F radical renders $Ag^{I}_2Ag^{II}(SO_3F)_4$ thermodynamically unstable with respect to products of thermal decomposition by both enthalpic and entropic factors.

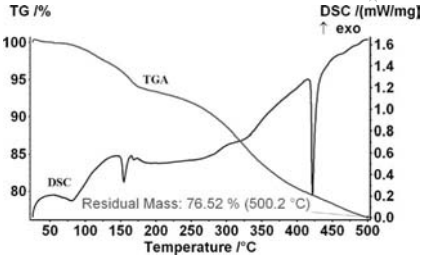

Figure 9. TGA/DSC plot of the thermal decomposition of $Ag^{I}_2Ag^{II}(SO_3F)_4$ (at 10 K min^{-1}).

To identify all crystalline products of thermal decomposition, XRD powder diffractograms were measured for samples of $Ag^{I}_2Ag^{II}(SO_3F)_4$ heated to 180 °C (453 K) and 500 °C (773 K), that is, the temperatures marking the end of the first and the second step of decomposition, respectively. The main products were identified as $AgSO_3F$ and Ag_2SO_4, respectively (Figure 10). This result suggests that $Ag^{I}_2Ag^{II}(SO_3F)_4$ decomposes thermally according to the following simplified reaction equations (6) and (7).

$$\text{I. } 1/3\ Ag_3(SO_3F)_4 \rightarrow AgSO_3F + 1/6\ (SO_3F)_2 \quad (6)$$

75–180 °C (theor. –13.8% mass)

$$\text{II. } AgSO_3F \rightarrow 1/2\ Ag_2SO_4 + 1/2\ SO_2F_2 \quad (7)$$

180–500 °C (theor. –21.2% mass)

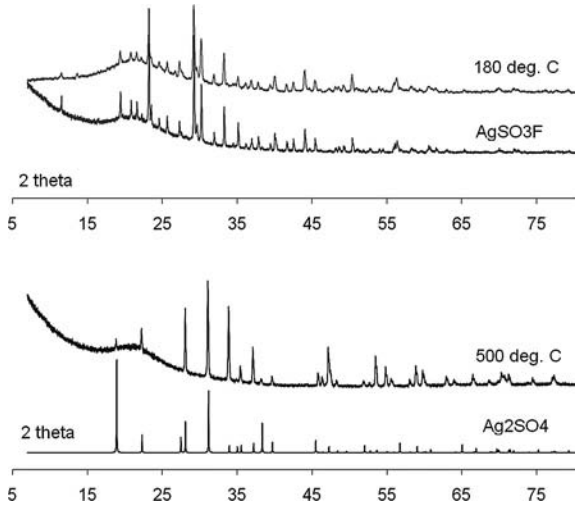

Figure 10. XRD powder diffractograms of the products of the first (top, 180 °C) and the second step (bottom, 500 °C) of the thermal decomposition of $Ag(I)_2Ag(II)(SO_3F)_4$.

Lack of the endothermic DSC peak at 435 °C corresponding to melting of AgF suggests that $AgSO_3F$ does not evolve SO_3 – see Equation (8) – as sometimes observed for ionic fluorosulfates.[23]

$$\text{III. } AgSO_3F \not\rightarrow AgF + SO_3 \quad (8)$$

The observed values of mass loss for both steps of thermal decomposition are much smaller than the theoretical values given above. The discrepancies indicate that the complex process of thermal decomposition is not completed at 500 °C (as clearly seen from the TGA profile) and it involves parallel processes that overlap on the temperature scale. At the time of the TGA/DSC/EGA measurement, $Ag^I_2Ag^{II}(SO_3F)_4$ (despite its high initial purity) must have been contaminated with a large amount of $AgSO_3F$ as a dead mass. Based on experimentally observed mass losses, the sample studied must have contained only approximately 40 wt.-% of $Ag^I_2Ag^{II}(SO_3F)_4$ and as much as approximately 60 wt.-% of $AgSO_3F$. Presence of $AgSO_3F$ [i.e., product of a facile exothermic thermal decomposition of inherently unstable $Ag^I_2Ag^{II}(SO_3F)_4$, step I], is not unexpected since the samples undergoing TGA/DSC/EGA measurements are conditioned for at least one hour before the beginning of the measurement in the stream of argon gas (precise mass stabilization is required for correct TGA experiment). Under such conditions the volatile $(SO_3F)_2$ product is dynamically removed while accelerating decomposition.

The EGA (a combination of MS and FTIR, Figure 11) helps to get additional insight into chemical reactions occurring during thermal decomposition. Mass spectra indicate that during the first step of decomposition a fragmentation of evolved $(SO_3F)_2$ takes place [signals at *m*/*z* ratio

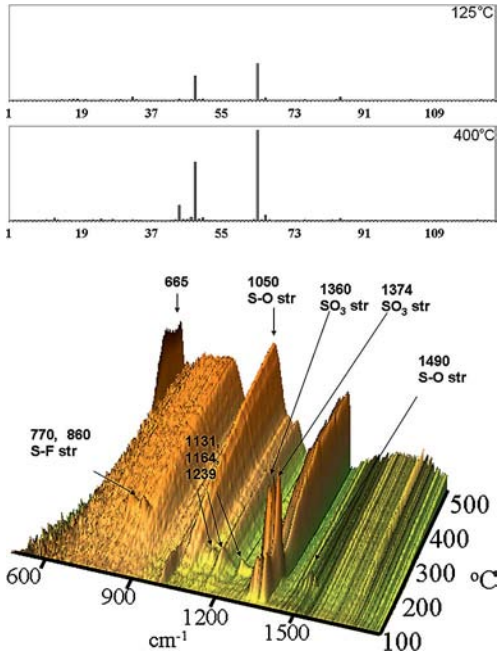

Figure 11. The mass spectra of gases evolved during thermal decomposition of $Ag^I_2Ag^{II}(SO_3F)_4$ at 125 (top) and 400 °C (middle) and the temperature dependence of the IR spectra of the evolved gases (bottom).

of 19 (F), 48 (SO), 64 (SO_2) and 67 (SOF)[24]] while the FTIR spectrum confirms the presence of bands assigned to S–O and S–F bonds (S–O stretching bands at 1050, 1360, 1374 and 1490 cm^{-1} and S–F stretching at 770 and 860 cm^{-1}).[25] During the second step of decomposition similar signals are seen in both MS and FTIR spectra, but the band at 1050 cm^{-1} (S–O stretching) and the band at 665 cm^{-1} (deformation mode), are now much stronger than the remaining ones.

Conclusion

The mixed-valent Ag^I/Ag^{II} compounds remain largely unexplored. Herein we have described the synthesis and detailed characterization of dark brown $Ag^I_2Ag^{II}(SO_3F)_4$, first prepared in the late 1970s.[2] This compound has a genuine mixed (frozen)-valent character[26] and it is a semiconductor of the Mott–Hubbard type. The infinite $\{Ag^{II}(SO_3F)_{2/2}{}^+\}$ chains (structurally analogous to the well-known AgF^+ chains[27]) are linked with additional fluorosulfate anions into $\{Ag^{II}(SO_3F)_{4/2+2/2}{}^-\}$ sheets present in the crystal structure of the title compound $Ag^I_2Ag^{II}(SO_3F)_4$, which behaves as an antiferromagnet with appreciable antiferromagnetic exchange within the $\{Ag^{II}(SO_3F)_{2/2}{}^+\}$ chains (J = –7.5 meV per pair of Ag^{II} centres); the DFT calculations reproduce the experimentally observed antiferromagnetism and additionally predict a very weak ferromagnetic exchange between the neighbouring chains. The large absolute value of intrasheet J shows that fluorosulfate monoanions are capable of transmitting antiferromagnetic superexchange between paramagnetic Ag^{II} centres almost as well as sulfate dianions.[6]

With just two examples known of compounds of $M^I_2Ag^{II}(SO_3F)_4$ stoichiometry (M^I = K, Ag), synthesis is now desired of other compounds of the types $M^I_2Ag^{II}(SO_3F)_4$, $M^IAg^{II}(SO_3F)_3$, $M^{II}Ag^{II}(SO_3F)_4$, $M^I_2Ag^{II}(SO_3F)_2(SO_4)$ and $M^{II}Ag^{II}(SO_3F)_2(SO_4)$. It would be interesting if 2D antiferromagnetism, similar to that seen for precursors of oxocuprate superconductors, could be observed for certain compositions.

Experimental Section

Synthesis: Due to the high reactivity of silver(II) compounds towards water all reactions were conducted under an argon atmosphere as provided by Labmaster DP glovebox from MBraun (O_2 < 1.0 ppm; H_2O < 1.0 ppm). All reaction vessels and all laboratory equipment having contact with the samples were made of Teflon or fluorinated ethylene propylene (FEP). The silver(I) fluorosulfate was obtained from commercial AgF (Sigma Aldrich) and an excess amount of HSO_3F (Sigma Aldrich). The solid residue was then rinsed with a mixture of trifluoroacetic acid (Sigma–Aldrich) and its anhydride (Sigma Aldrich). The reaction between $AgSO_3F$ and $BrSO_3F$ typically on a 0.5–1.0 g scale was conducted for 72 h using a HF line made of fluoropolymers. Volatile products of the reaction were removed from the HF line using a vacuum pump. The product was analyzed as obtained. $Ag_3(SO_3F)_4$ is black in appearance but grinding in agate mortar reveals its true dark brown colour, much darker than that of $Ag(SO_3F)_2$ or of AgF_2.

The dark red $BrSO_3F$ substrate was obtained by reacting an equimolar mixture of Br_2 and $(SO_3F)_2$ for 72 h.[28]

Structure Solution and Refinement: The cell indexation was performed by X-Cell[29] implemented in the Materials Studio package.[30] Multiphase Le Bail decomposition and Rietveld structure refinement (Figure 12) were performed in Jana2006. The structure of the title compound was solved by direct methods in Expo2004 using reflex intensities obtained from Jana2006. For a correct description of the complex background, 30 Legendre polynomials were used. The angle and distance uncertainties were obtained after application of Bérar's correction.[31]

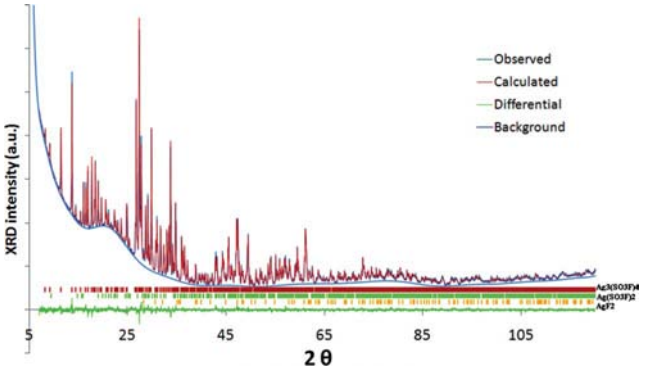

Figure 12. Experimental X-ray powder diffractogram of $Ag^{I}_2Ag^{II}(SO_3F)_4$, its decomposition to contributions from the crystalline phases and background, and the differential curve.

Further details on the crystal structure investigation may be obtained from the Fachinformationszentrum Karlsruhe, 76344 Eggenstein-Leopoldshafen, Germany (Fax: +49-7247-808-666; e-mail: crysdata@fiz-karlsruhe.de), on quoting the depository number CSD-422417.

Instrumental: IR spectra were measured using a VERTEX 80V IR spectrometer from Bruker with AgCl windows used for the mid-IR range (500–7500 cm^{-1}) and polyethylene windows for the far-IR (50–650 cm^{-1}) range. Raman spectra were measured using a Horiba Jobin Yvon LabRam-HR Raman microspectrometer with 632.8 nm He:Ne laser exciting beam. Si was used as a reference for setting of the zero shift. X-ray powder diffraction measurements were conducted using a D8 Discover diffractometer from Bruker equipped with Cu cathode and parallel-beam setting provided by Göbel mirrors. Samples were closed under an argon atmosphere in quartz capillaries (Hilgenberg GmbH, Ø = 0.3 mm, wall thickness 0.01 mm). The 62 h measurement covered the 2-theta range of 3–120°. Magnetic measurements were conducted by a superconducting quantum interference device magnetometer MPMS-XL-5 from Quantum Design equipped with a 50 kOe magnet. Magnetization measurements were conducted in both ZFC and FC regimes for a sample sealed inside a quartz tube in a magnetic field of 1000 Oe between 2 and 390 K. The data were corrected for temperature-independent diamagnetism due to the closed atomic shells as estimated from Pascal's tables.[32] ESR spectra were obtained using a ESP 300E spectrometer (frequency 9.5 GHz; the X band) from Bruker for samples sealed under an Ar atmosphere inside a 4 mm-thick quartz capillary. Thermal analysis was performed using a STA 409PG TGA/DSC analyzer from Netzsch coupled with an Aëolos QMS 403C mass spectrometer (Netzsch) and a VERTEX 80v IR spectrometer (Bruker) for EGA. Samples were loaded into alumina crucibles under an argon (99.9999%) atmosphere. The experiment was conducted in the temperature range of 30–500 °C (303–773 K) at the heating rate of 10 K min^{-1}. Both transfer lines were preheated to 200 °C to avoid condensation of residues. The silver content was determined using a method by Pendse[33] [precipitation of disilver(I) chromate]. The method shows an error margin of less than 1%. An alternative method published by Tradwell[34] (precipitation of metallic silver during reduction with H_2O_2) was attempted but found unreliable while using reference $AgNO_3$ samples. The sulfur and fluorine content was determined using the Schöniger method[35] at a detectability level of 0.2 wt.-% and a typical uncertainty of 0.3 wt.-% for each element. Two independent analyses were performed with differences between the measurements reaching no more than 0.2 wt.-% for each element. The numbers shown in this work are the mean of the two values.

DFT Calculations: Solid-state density functional theory (DFT) calculations were performed using the VASP code[36] with the projector-augmented wave method (PAW)[37] as implemented in the MedeA package. For the exchange-correlation part of the Hamiltonian, the local density approximation (LDA) in its LSDA (local spin density approximation) variant was applied, since we have noticed previously that LDA allows for much better reproduction than GGA of many important parameters of related $AgSO_4$.[38] Due to the very large size of the unit cell (92 atoms) and rather low symmetry of the magnetic models, the geometry optimization (i.e., the cell and atomic parameters) was not performed; for the same reason all calculations were performed in real space. The electronic iterations convergence was set to 10^{-7} eV per atom by using the standard blocked Davidson algorithm. The Γ-centred k-point mesh automatically generated through the Monhorst–Pack grid of $4 \times 2 \times 1$ yielded 6 unique k points. The valence electrons were described by plane waves with a kinetic energy cutoff of 600 eV, yielding a satisfactory convergence of total energy. The same parameters were used for the single-point energy, spin density, band structure and DOS calculations on a $1 \times 1 \times 1$ experimental unit cell.

To derive the electronic and magnetic structure of $Ag_3(SO_3F)_4$, both the spin-polarized LSDA and LSDA+U single-point calculations were performed. To mimic the strongly correlated nature of the 4d electrons of Ag and the interacting p electrons of the bridging "oxide anions" (within the superexchange Ag^{II}–OO–Ag^{II} path), the value of the Coulomb integral U was set to 4 eV and Hund's exchange J to 1 eV for both of these ions; the respective values for S(3p) electrons were 2 and 1 eV, thus allowing direct comparison with results obtained earlier for $AgSO_4$.[6,38] The Mott–Hubbard U was not applied to the formally closed-shell ($4d^{10}$) Ag^{I} cations. We found that inclusion of U for Ag^{I} leads to severe overestimation of magnetic superexchange constant J. Two different schemes of magnetic ordering were tested in single-point energy calculations: one ferromagnetic (FM) with FM intrachain and FM interchain coupling, and one antiferromagnetic (AFM) with AFM intrachain and FM interchain coupling as well as a nonmagnetic cell. The AFM ordering corresponds to a global energy minimum at both LSDA and LSDA+U levels of theory. The sign of interchain superexchange was obtained by means of calculations for a modified $2 \times 1 \times 1$ supercell of $Ag_3(SO_3F)_4$ in which the diamagnetic $Ag^{I}_2(SO_3F)^+$ cations were substituted with Li^+ cations to reduce the size of the model from 184 (overrunning the VASP limit) down to 136 atoms [structural integrity of the $Ag(SO_3F)_3^-$ layers was preserved].[20]

Acknowledgments

The project "Quest for superconductivity in crystal-engineered higher fluorides of silver" is operated within the Foundation for Polish Science "TEAM" Program co-financed by the EU European

Regional Development Fund. This work has been partly supported by the Slovenian Research Agency (ARRS) within the research program P1-0045 Inorganic Chemistry and Technology. Calculations have been performed at ICM supercomputers.

[1] A few mixed-valent (1+,2+) fluorides of Ag have recently been predicted from DFT calculations: W. Grochala, *J. Mol. Model.* **2011**, DOI: 10.1007/s00894-010-0949-4.
[2] P. C. Leung, F. Aubke, *Inorg. Chem.* **1978**, *17*, 1765–1772.
[3] Q. M. Wang, H. K. Lee, T. C. W. Mak, *New J. Chem.* **2002**, *26*, 513–515.
[4] Q. M. Wang, T. C. W. Mak, *Chem. Commun.* **2001**, 807–808.
[5] Z. Mazej, E. Goreshnik, *Pacifichem – The International Chemical Congress of Pacific Basin Societies*, Honolulu, USA **2010**.
[6] P. J. Malinowski, M. Derzsi, B. Gaweł, W. Łasocha, Z. Jagličić, Z. Mazej, W. Grochala, *Angew. Chem.* **2010**, *122*, 1727; *Angew. Chem. Int. Ed.* **2010**, *49*, 1683–1686.
[7] W. Grochala, R. Hoffmann, *Angew. Chem.* **2001**, *113*, 2816; *Angew. Chem. Int. Ed.* **2001**, *40*, 2742–2781.
[8] P. Malinowski, M. Derzsi, Z. Mazej, Z. Jagličić, P. J. Leszczyński, T. Michałowski, W. Grochala, submitted to *Eur. J. Inorg. Chem.* **2011**, 2499–2507; preceding paper.
[9] V. Petriček, M. Dušek, L. Palatinus, *Jana2006*, *The Crystallographic Computing System*, Institute of Physics, Praha, Czech Republic, **2006**.
[10] A. Altomare, R. Caliandro, M. Camalli, C. Cuocci, C. Giacovazzo, A. G. G. Moliterni, R. Rizzi, *J. Appl. Crystallogr.* **2004**, *37*, 1025–1028.
[11] W. Grochala, *Phys. Status Solidi B* **2006**, *243*, R81–R83.
[12] I. D. Brown, D. Altermatt, *Acta Crystallogr., Sect. B* **1985**, *41*, 244–247.
[13] P. J. Malinowski, T. Michałowski, W. Grochala, unpublished data.
[14] J. R. Dalziel, R. D. Klett, P. A. Yeats, F. Aubke, *Can. J. Chem.* **1974**, *52*, 231–239.
[15] K. Momma, F. Izumi, *J. Appl. Crystallogr.* **2008**, *41*, 653–658.
[16] G. A. Lawrance, *Chem. Rev.* **1986**, *86*, 17–33.
[17] C. S. Alleyne, K. O. Mailer, R. C. Thompson, *Can. J. Chem.* **1974**, *52*, 336–342.
[18] J. C. Boner, M. E. Fisher, *Phys. Rev. A* **1964**, *135*, A640–A658.
[19] Ag^{II} forms substantial covalent bonds even to F^{-1} anion: W. Grochala, R. G. Egdell, P. P. Edwards, Z. Mazej, B. Žemva, *ChemPhysChem* **2003**, *4*, 997–1001.
[20] The antiferromagnetic interchain coupling is weak compared to the intrachain coupling, with the interchain exchange parameter smaller from intrachain *J* by over one order of magnitude; this feature renders $Ag_3(SO_3F)_4$ a quasi-1D antiferromagnet at room temperature.
[21] J. Köhler, *Angew. Chem.* **2010**, *122*, 3180; *Angew. Chem. Int. Ed.* **2010**, *49*, 3114–3115.
[22] C. W. F. T. Pistorius, *J. Chem. Phys.* **1967**, *46*, 2167–2171.
[23] J. Gaubeau, J. B. Milne, *Can. J. Chem.* **1967**, *45*, 2321–2326.
[24] Other signals are also present: 50 (H_2SO_2), 66 (H_2SO_3), 85 ($HSO_2 \times HF$); presence of H comes from the water content of the carrier Ar gas.
[25] The literature values for the SO_3F radical are 1178, 1056, 839, 604, 534 and 369 cm^{-1} (G. W. King, C. H. Warren, *J. Mol. Spectrosc.* **1969**, *32*, 121–137), those for the strongest IR-active bands of SO_2F_2 are 1502, 1269, 855 and 848 cm^{-1} (see www.nist.gov), whereas those for SO_3 are 1391, 1068, 529 and 495 cm^{-1} (see V. E. Bondybey, J. H. English, *J. Mol. Spectrosc.* **1985**, *109*, 221–228, and references cited therein). Emission of $S_2O_5F_2$, ill-characterized in the literature, cannot be excluded.
[26] As a referee correctly reminded us, mixed-valent compounds are worth characterizing with methods such as NIR-visible-UV reflectance, X-ray photoelectron spectroscopy (XPS) and X-ray absorption near-edge structure (XANES), as well as electric conductivity measurements. Unfortunately, the last ones present a formidable challenge as far as strongly oxidizing compounds of Ag^{II} are concerned: W. Grochala, P. P. Edwards, *Phys. Status Solidi B* **2003**, *240*, R11–R14. It is difficult to suggest a material for electrodes in any contact measurement, as compounds of Ag^{II} easily oxidize even metallic gold.
[27] W. J. Casteel, G. Lucier, R. Hagiwara, H. Borrmann, N. Bartlett, *J. Solid State Chem.* **1992**, *96*, 84–96.
[28] F. Aubke, R. J. Gillespie, *Inorg. Chem.* **1968**, *7*, 599–603.
[29] M. Neumann, *J. Appl. Crystallogr.* **2003**, *36*, 356–365.
[30] Materials Studio 4, Accelrys, Inc. **2007**, San Diego, USA.
[31] J.-F. Bérar, P. Lelann, *J. Appl. Crystallogr.* **1991**, *24*, 1–5.
[32] O. Kahn, *Molecular Magnetism*, VCH, New York, **1993**.
[33] G. P. Prendse, H. D. Bhargava, B. R. Sant, *Fresenius J. Anal. Chem.* **1958**, *160*, 188–189.
[34] F. P. Tradwell, T. Hall, *Anal. Chem.* **1955**, *640*, 95–98.
[35] See: A. M. G. Macdonald, *Analyst* **1961**, *86*, 3–12, and references therein.
[36] G. Kresse, J. Furthmüller, *Phys. Rev. B* **1996**, *54*, 11169–11186.
[37] P. E. Blöch, *Phys. Rev. B* **1994**, *50*, 17953–17979.
[38] M. Derzsi, J. Stasiewicz, W. Grochala *J. Mol. Model.* **2011**, DOI: 10.1007/s00894-010-0950-y.

Received: February 1, 2011
Published Online: April 26, 2011

